Supporting information for the Communication:

The poly dA helix: A new structural motif for high performance DNA based molecular switches

Saikat Chakraborty[‡], *Suruchi Sharma*[‡], *Prabal K Maiti*[†] *and Yamuna Krishnan**[‡]

[‡]National Centre for Biological Sciences, Tata Institute of Fundamental Research, GKVK, Bellary Road, Bangalore 560 065, India

[†]Centre for Condensed Matter Theory, Department of Physics, Indian Institute of Science, Bangalore 560 012, India

CD and UV melting Studies:

To investigate the nature of the stabilizing interactions in d$\mathbf{A}_{15}$, d$\mathbf{A}_{15}$ samples at both acidic and neutral pH were thermally denatured and followed as a function of temperature both by circular dichroism (CD) and UV (SI Figure 1). For acidic pH, samples were made as described in the main text at several concentrations ranging from 1 μM to 10 μM in 5 mM phosphate buffer, pH 3.0. For neutral pH, samples were made at 2 μM strand concentration in 5 mM phosphate buffer, pH 7. All the samples were investigated in the temperature regime of 20ºC to 100ºC following the absorbance at 260 nm by UV spectrometry or circular dichroism at 262 nm.

At neutral pH, d$\mathbf{A}_{15}$ evidences a weakly structured form as seen from the broad and non-cooperative melt in both UV and CD melting profiles (SI Figure 1B and C). However, the melting temperatures were different as obtained from UV ($T_{1/2}$= 46ºC) and CD ($T_{1/2}$=53ºC). This is due to the fact that two different properties of the complex are followed by UV (base stacking) and CD (chirality). As shown in the main text (Figure 2B) the 280 nm band in CD observed at pH 7.0 arises from a forbidden (n-π*) transition which is observable when water is excluded from the bases, as happens in a stacked conformation (s1). This indicates that d$\mathbf{A}_{15}$ is structured at neutral pH, stabilized majorly by stacking interactions. The loss of this band on heating implies the loss of stacking interactions. This is in line with previous findings (s2) on single helices of poly d**A** that suggest that stacking interactions are the main driving forces in the poly d**A** single helix.

At pH 3.0, however, d$\mathbf{A}_{15}$ shows a much better defined sigmoidal thermal transition both in UV and CD indicating a structure that is cooperatively held (Figure 5B, SI Figure 1A). There is a strong dependence of $T_{1/2}$ on strand concentration as can be seen from the

melting profiles consistent with the duplex being an intermolecular complex. Extracting thermodynamic parameters from these melting profiles is not possible as it is well documented that at acidic pH, adenosine homopolymers undergo depurination at elevated temperatures. Thus, these thermally induced transitions cannot be considered reversible.

SI Table 1. Concentration dependence of the duplex thermal stability as probed by CD.

Concentration (μM)	$T_{1/2}$ (in °C)
2	83
5	88
10	90

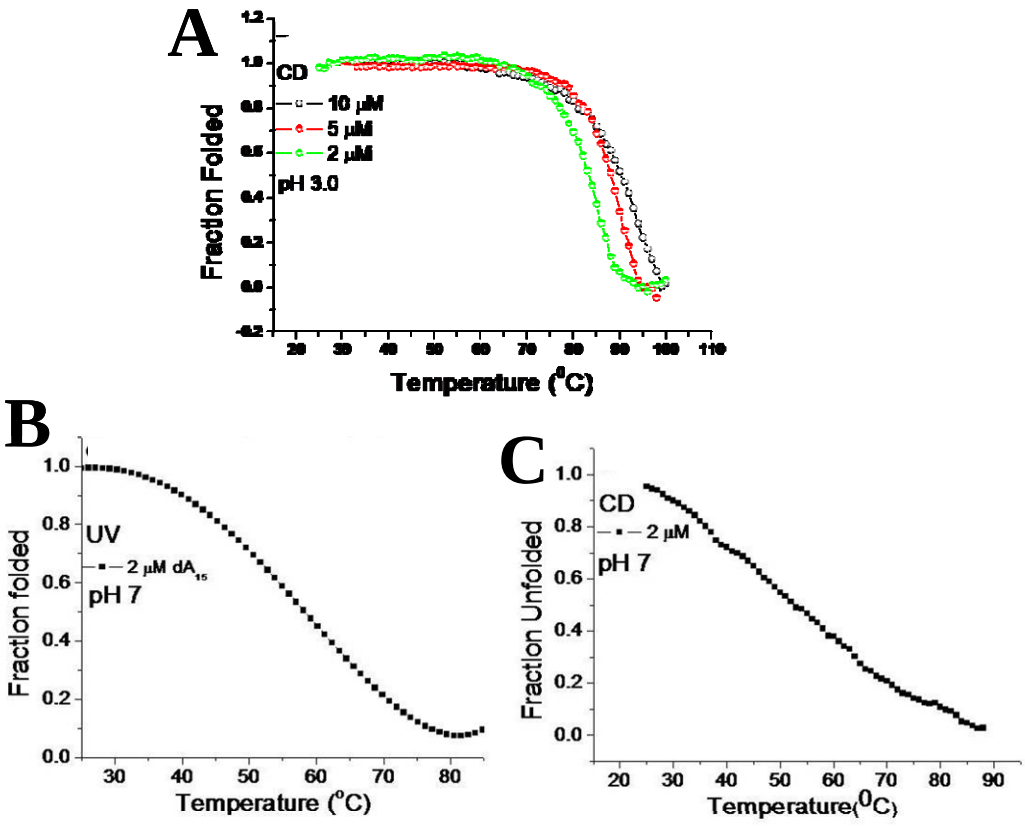

SI Figure 1: (**A**) CD thermal melts of the poly d**A** duplex in 10 mM sodium phosphate buffer, pH 3 (**B**) and (**C**), melting of poly d**A** at pH 7 probed by UV and CD respectively.

Salt dependence:

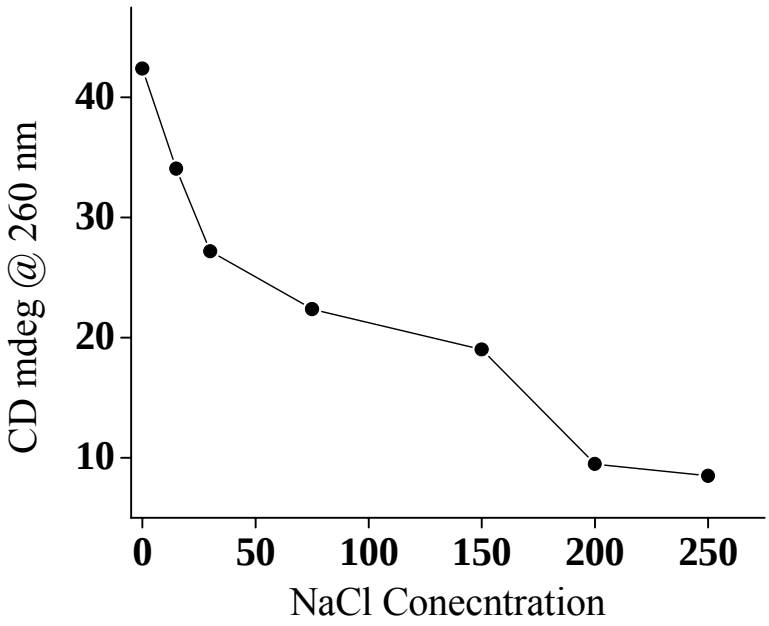

SI Figure 2: Effect of salt on CD spectra of d**A**$_{15}$ duplex in unbuffered pH 3 water.

Fluorescence experiments:

Fluorescence spectra of TAMRA-TAMRA self quenching was recorded on a JASCO J-815 Spectropolarimeter equipped with a fluorescence detector and in 10 mm path length quartz cuvette. Prior to acquisition samples were diluted 5 fold in the cuvette. Samples were excited at 520 nm and emission was recorded between 540-700 nm, at scan rate of 1 nm/sec. The working formula used for the calculation of the distances is the following:

$$E=1- f_{D/A}/f_D =R_o^6/ (R^6+R_o^6) \text{ …….(1)}$$

Where $f_{D/A}$= fluorescence intensity in the presence of both the donor and acceptor; f_D = fluorescence intensity of the donor only; E= efficiency of energy transfer; R_o= Förster distance; and R= distance between the donor and acceptor. The distances between the labeled strands were calculated using fluorescence intensity of the complex at pH 3.0 ($f_{D/A}$) and the fluorescence intensity of samples at pH 7 (f_D). The Förster distance (R_o) for TAMRA–TAMRA self-quenching was 44 Å as described previously (s4). Estimates of the relevant distances were obtained from the MD simulated model of the poly d**A** duplex incorporating the linkers.

As a control for alteration in TAMRA fluorescence due to environmental effects such as pH change and structural effects samples were prepared at total strand concentration 5 μM with 50:1 d$\mathbf{A}_{15}$:5′-TAMRA-d$\mathbf{A}_{15}$ such that every TAMRA-d$\mathbf{A}_{15}$ strand is statistically incorporated into a duplex with only one TAMRA label. When the pH of this sample is changed from 7 to 3.0 we observed ~17% decrease in fluorescence which is used as a correction factor for doubly-labeled TAMRA duplexes which yields the contribution purely due to self-quenching (see SI Fig 3B and main text). In order to confirm that this quenching occurs because of proximal position of the fluorophores in the duplex and not by the dimer formation between the fluorophores we measured the anisotropy of the fluorophores at pH, 3 and 7. Anisotropy trajectories of the fluorophores at different pH, shown in the SI Figure 3C, indicates that the fluorophores are rotating freely confirming that self-quenching is solely due to proximal position of fluorophores due to parallel duplex formation.

To calculate the distance between the two like ends of the duplex TMR-DABCYL fluorophore-quencher pair was used with R_o of 26 Å (s4). Dually labelled duplex was made with a 1:50 TMR-d$\mathbf{A}_{15}$: DABCYL-d$\mathbf{A}_{15}$. This ensured that every 3′-TMR-d$\mathbf{A}_{15}$ was paired with a Dabcyl d$\mathbf{A}_{15}$. Homo-Dabcyl-duplexes, which are the major species, are fluorescently silent and do not affect the experiment. 1:50 3′-TMR-d$\mathbf{A}_{15}$:d$\mathbf{A}_{15}$ served as a control for donor-only labelled duplex (f_D). The fluorescence intensity of the control (f_D) at pH 3 was normalized to the value of intensity upon giving the sample a pH jump to pH 7, thus correcting for any concentration effects. Thus the fluorescence intensity in the presence of the quencher in the doubly labelled duplex (f_{DA}) at pH 3 was measured and normalized as described. The efficiency of energy transfer and hence the distance is calculated from the equation (1).

Effect of pH on free TMR (tetramethylrhodamine-5-maleimide) was also checked as shown in Figure 3D. The fluorescence emission spectra of 500 nM free TMR in 1 mM NaCl, pH 7 recorded using 550 nm excitation and emission between 560 nm-650 nm. The pH was altered incrementally by adding requisite amount of 0.5 mM phosphate buffer of desired pH and spectra recorded. The spectrum at any given pH was normalized to its value at pH 7 which eliminated differences due to experimental variations in

concentration. At pH 3, 4 and 5 14%, 13% and 10 % quenching at 575 nm was observed compared to pH 7, respectively.

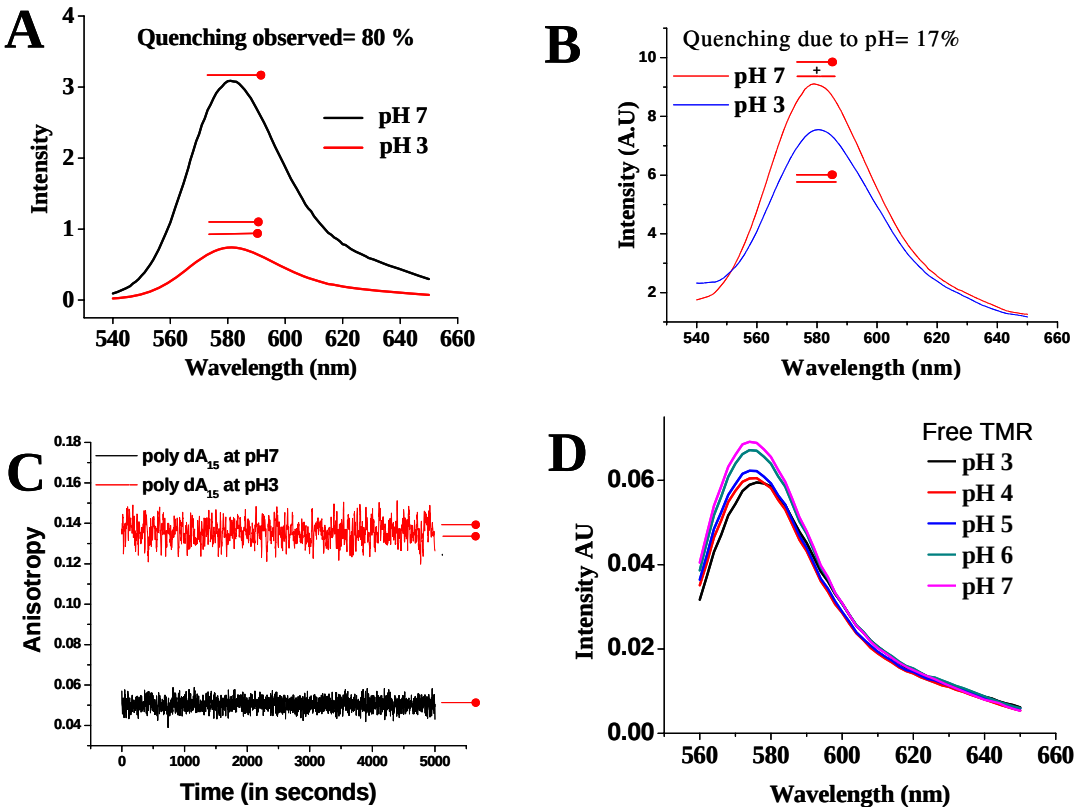

Figure 3: (A) Fluorescence self-quenching of 5′-TAMRA-d**A**$_{15}$ in the duplex (pH 3) and single helical (pH 7) states **(B)** Control fluorescence experiment on 50:1 d**A**$_{15}$:5'-TAMRA-d**A**$_{15}$ at pH 3 and pH 7 showing quenching due to change in pH. (C) Anisotropy time series of duplexed and single helical d**A**$_{15}$. (**D**) Control fluorescence experiment showing quenching due to pH decrease of free TMR.

pH titration:

In order to follow the pH induced structural transition in poly d**A** kinetically, we formed two samples of poly d**A** of 5 μM at pH 3 and pH 7 in unbuffered solutions. We increased the pH of pH 3 solutions by 0.2 pH units incrementally till pH 7. Similarly we decreased the pH of the solution at pH 7 by 0.2 pH units until it reaches pH 7. Structural transition in these two titrations was visualized by circular dichroism at 262 nm. CD profiles at different pH are shown in SI Figure 4. This indicates the reproducibility in conformational switching in this system.

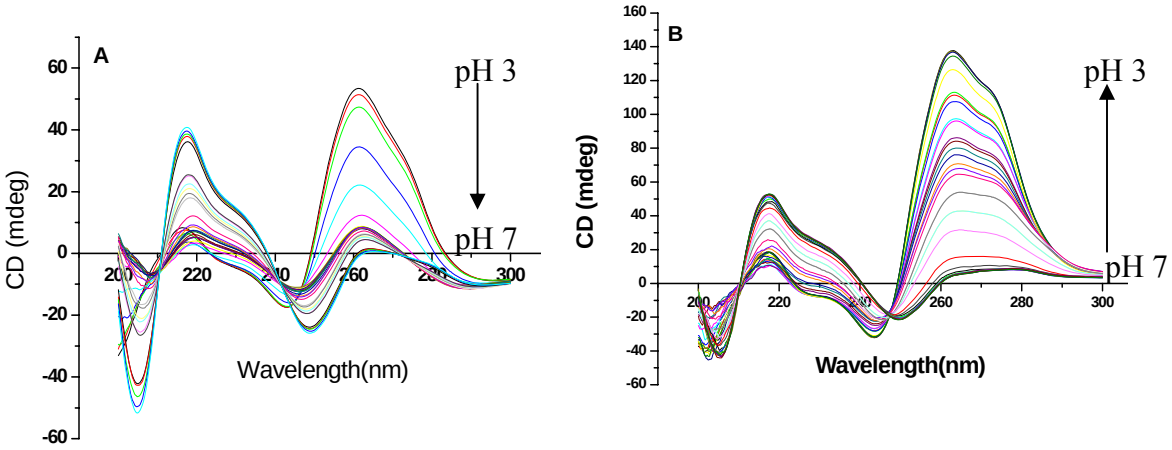

SI Figure 4: A) structural transition of d$\mathbf{A}_{15}$ from pH 3 to pH 7. B) Structural transition from pH 7 to pH 3. Transitions are brought about by adding 5 µL of 0.01 N HCl or NaOH.

Switching and cycling:

As mentioned in the main text, cycling between single stranded helix to double stranded form by the poly d**A** was probed by circular dichroism at suitable wavelength. Samples of 5 µM d$\mathbf{A}_{15}$ were prepared in unbuffered solution at pH 7 and pH of the solution was changed to pH 3 and vice versa by alternate addition of 0.01N acid and base. Double helix formation was probed by CD at 262 nm where the duplex shows high positive CD and the single helix shows negligible CD. As shown in SI Figure 5, over ten cycles we observed efficient cycling by poly d**A**.

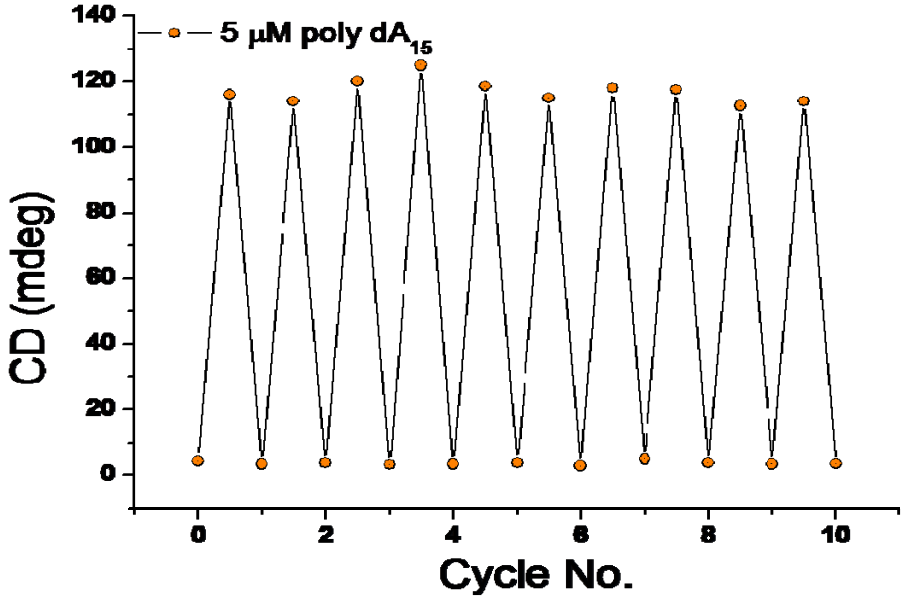

SI Figure 5: Conformational switching of poly d**A**$_{15}$ between single and double helical forms visualized by CD at 262 nm, by alternate addition of acid and base respectively.

Gel Electrophoresis

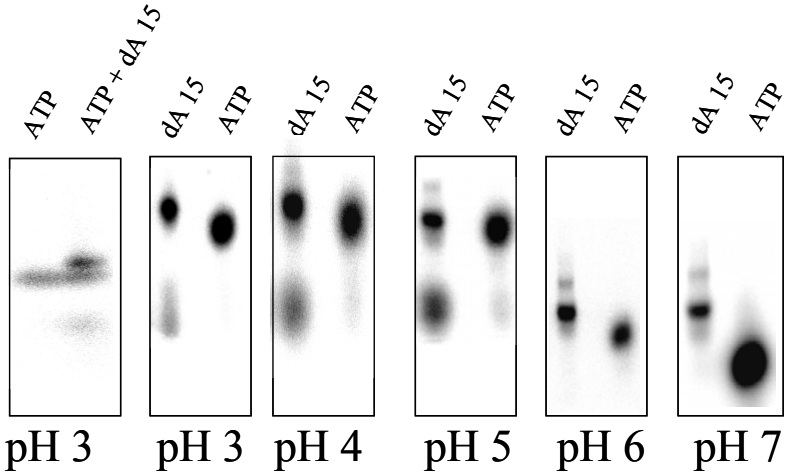

SI Figure 6: Gel images of P^{32}-labeled poly d**A**$_{15}$ (d**A**$_{15}$*) in comparison with P^{32}-ATP (ATP*) to show that the bands of interest are not due to the latter. From left: Gel showing Lane 1: ATP* alone; Lane 2: an externally added amount of ATP* to dA$_{15}$* at pH 3. Gels showing Lane 1: dA$_{15}$*, Lane 2: ATP* at the pH indicated below. Electrophoresis was performed in 15% native PAGE in 1X Robinson- Britton buffer of required pH at 20°C at

10 V/cm and visualized using PhosphorImager**.** Note that migration of ATP* changes from pH 6 to pH 5 due to protonation on N1 of adenine.

Figure 2A (main manuscript) showed that d$\mathbf{A}_{15}$ adopted two forms having different electrophoretic mobilities as a function of pH. In order to ensure that the observed bands are not due to residual P^{32}-ATP used for labeling d$\mathbf{A}_{15}$, P^{32}-ATP was mixed with radiolabelled d$\mathbf{A}_{15}$ at the relevant pH and loaded in the gel (see leftmost panel, SI Figure 6). This was also done at various indicated pH values (see remaining panels) and it was noted that both bands observed were due to labeled d$\mathbf{A}_{15}$ and not P^{32}-ATP.

1D and 2D NMR

SI-Figure 7A shows NOE crosspeaks between thymine H6 and its corresponding sugar H1' and H2'/H2". The presence of a single crosspeak evidences the formation of a single conformational species in bulk at pH 4. SI-Figure 7B shows NOE crosspeaks and the associated NOE walk for the adenine H8 and sugar H2'/H2". The NOE connectivities between these protons are commensurate with a parallel stranded dTA_6 duplex. SI-Figure 7C shows the region of 1D spectrum corresponding to the adenine H2 protons. It was observed that several H2 protons were split with a constant ^3J coupling of ~7.5 Hz indicating the presence of another proton in the same spin system. Importantly, these H2 protons showed no splitting at pH 8. It has been shown in other N1-protonated pyridiazine systems in water, that at acidic pH, protonation at N1 sites splits the H2 protons due $^3J_{H\text{-}H}$ coupling (s5). This therefore clearly points to N1 protonation in the dTA_6 duplex at pH 4. Importantly N1 protonation rules out A-A base-pairing via the reverse Watson Crick faces of adenine and supports base-pairing via the reverse Hoogsteen faces (See SI-Figure 8). This is highly consistent with the MD simulated duplex structure.

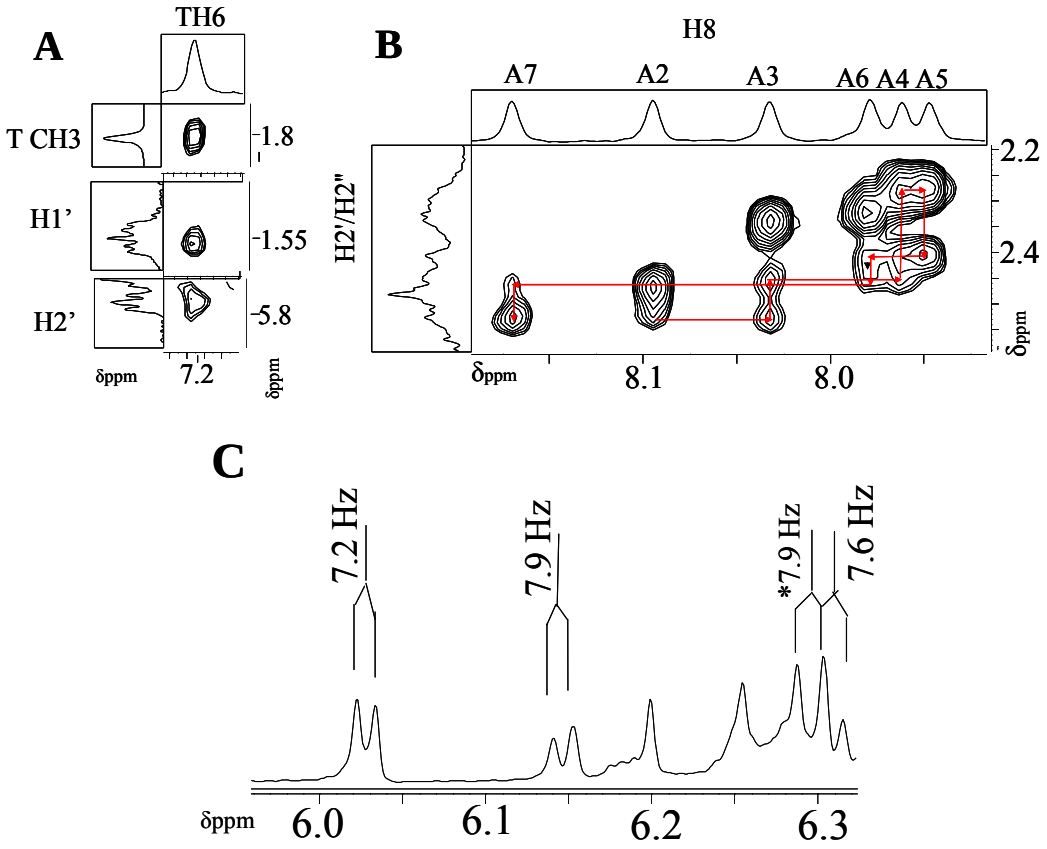

SI Figure 7. A) Partial NOESY spectrum in a 500 MHz Bruker NMR spectrometer showing NOE crosspeaks of thymine H6 with sugar protons establishing presence of a single thymine, characteristic of a unique conformational population. **B)** Partial NOESY spectrum of the NOE walk corresponding to H2′/H2″-Adenine H8 contacts in 1 mM dTA_6, pH 4, 50 mM d3-Na-acetate. C) 1D spectrum of dTA_6, pH 4, d3-Na-acetate showing splitting of several adenine H2 protons characteristic of N1 protonation at these positions. Also shown are the corresponding ^{3}J-values; '*' indicates that this value was obtained from the D_2O exchanged spectrum (data not shown) which showed these peak separations with greater clarity.

Establishing Reverse- Hoogsteen base pairing scheme:

In the literature only two kind of A-A homo base pairs have been reported in the context of A-containing sequences that form parallel DNA duplexes (s6). These are shown below in SI-Figure 8.

The reverse Watson-Crick mode of base pairing can readily be eliminated due to the fact that N1 in dTA6 is protonated. Protonation at the N1 site cannot support reverse WC base pairing as N1 has to be unprotonated in order to function as an H-bond acceptor for the

N6 amino group (See SI-Figure 8A). This effectively means that the AH^+-H^+A base pairing can only be of the reverse Hoogsteen type. Moreover, the nucleobase positioning of the reverse Hoogsteen faces is compliant with simultaneous N1 protonation on both bases with the $N1^+$ sites electrostatically interacting with the phosphate backbone of the opposite strand. Furthermore, in the 1D- spectrum at 800 MHz, we observe two kinds of NH_{2b} resonances and this is consistent with the reverse Hoogsteen type base-pairing where the two NH_2 protons are H-bonded to two different chemical entities.

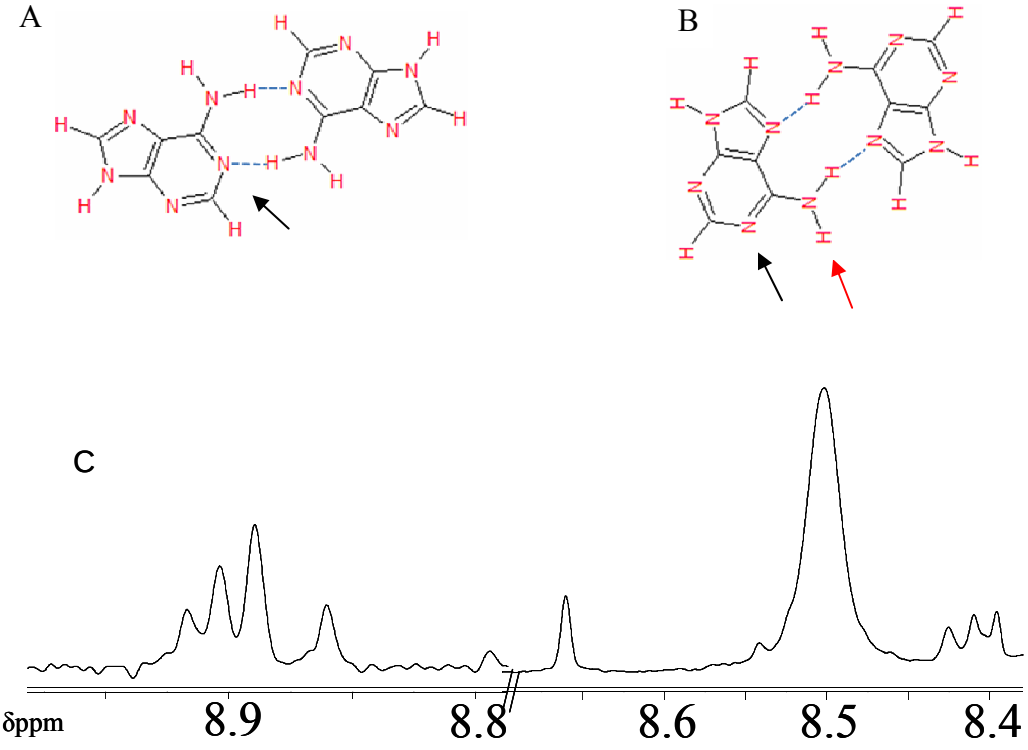

SI-Figure 8: Schemes predicted for both types of A-A base pairs in parallel duplexes. (A) Adenines base-pairing via their reverse Watson-Crick faces where N1 (indicated by black arrow) is involved in H-bonding with N6H. B) Adenines base-pairing via their reverse Hoogsteen faces where N1 (indicated by black arrow) is not involved in H-bonding and hence available for protonation; and N6H (indicated by red arrow) can interact with $^-$O-P as seen in poly r(AH^+-H^+A). C) Partial 1D spectrum (800 MHz Bruker) showing 2 different adenine NH_{2b} protons.

Molecular Dynamics Study:

*Poly d**A** single helix*: The poly d**A** single strand was built in NAMOT 2 software and MD simulations performed using AMBER9 (s7) with the all-atom AMBER03 force field. SI Figure 9 shows the structure of the helix before and after MD simulation.

*Poly d**A** double helix*: The starting conformations for the simulations were generated in the following way. The parallel Hoogsteen AH^+-H^+A base pair (Leontis/Westhof Classification Legend 8 and Saenger classification II) with trans glycosidic bond orientation was made as described for the poly r**A** double helix using NAMOT 2 [s8] and then multimerized to create a double helix. The pitch (30.4 Å) and rise per base pair (3.8 Å) was maintained as described for the poly r**A** double helix [s3]. The adenine protonation was modeled by adding H1 hydrogen to the N1 atom. Each adenine in every base pair was protonated. Added hydrogen for the protonated base was assigned as AMBER type H5. The partial charges for the protonated adenosine were obtained using the following procedure. Adenosines were protonated at N1 position and dimethyl phosphate molecules were optimized at HF/6-31G(d) level of theory using Gaussian program package [s9]. The Electrostatic surface potential (ESP) of the two molecules were used for calculating the partial charges of nucleotides (protonated DA3, DA, DA5). Antechamber [s10] module of AMBER suite of programs was used to extract the ESP charges and a two stage fitting was done using the Amber's restrained electrostatic potential (RESP) [s7] where the inter-molecular charge restraints and equivalency of atoms are considered as in Cieplak *et al* [s11]. This structure was the starting point for the MD simulations of the protonated poly d**A** double helix (See SI figure 13A). An additional simulation was also run on a poly d**A** double helix without protonation of adenosines as a control (See SI Figure 13).

MD simulation protocol:

Using the LEaP module in AMBER, the DNA structure was immersed in a water box using the TIP3P model for water [s12]. The box dimensions ensured a 10 Å solvation shell around the DNA structure. In addition, some water molecules were replaced by Na^+ ions to neutralize the negative charge on the DNA phosphates in the case of the un-protonated double helix. The system was then subjected to the equilibration protocol as outlined previously [s13-15]. All MD simulations used the AMBER9 software package

with the all-atom AMBER03 force field [s15]. The electrostatic interactions were calculated with the Particle Mesh Ewald (PME) method using a cubic B-spline interpolation of order 4 and a 10^{-4} tolerance set for the direct space sum cutoff [s15-16]. A real space cut off of 9 Å was used both for the electrostatic and van-der Waals interactions with a non-bond list update frequency of 10. It is important to note that in the constructed model of the poly d**A** duplex, the AH^{+}-$H^{+}A$ base pairs were perfectly planar with 0˚ tilt to the perpendicular to the helix long axis (See SI-Figure 13A). We used a distance restraint of 1.9 Å between the hydrogen of the base (N6-H1) and the oxygen attached to phosphate (O2P) for each base as seen in the AH^{+}-^{+}HA base pairing in the fiber diffraction structure of poly r**A**.

MD simulation on single stranded poly d**A**:

It is generally assumed that the helical structure of nucleic acids are formed from double stranded regions stabilized by base paring, following the classical Watson-crick base pairing model. In the absence of base pairing the random coil is usually considered as the alternative structure. However, at pH 7 both poly r**A** as well as poly d**A** show very high Circular Dichroism which is also distinct from the random coil signature. Further, they exhibit hyperchromicity in UV with increasing temperature.

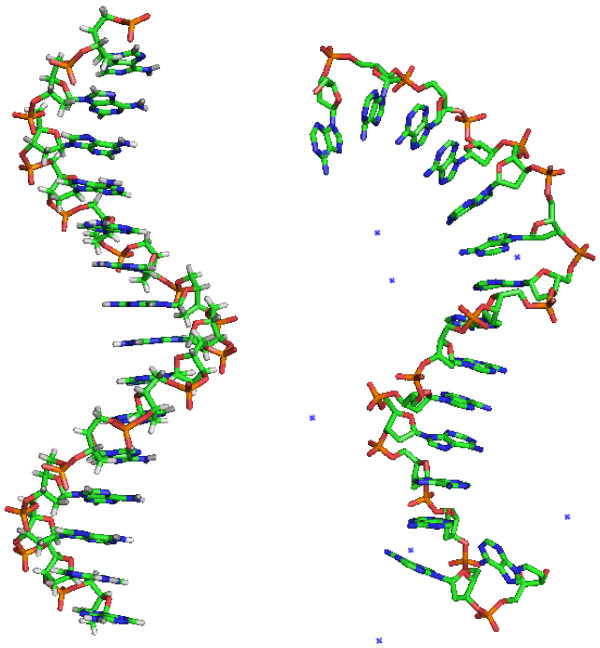

SI-Figure 9: A) Starting conformer of the single stranded poly d**A** constructed for MD simulation. B) The poly d$\mathbf{A_{15}}$ single helix obtained after 20 ns simulation. The single helix is 9-fold with a helix pitch of ~26 Å and a rise per base ~2.9 Å. The adenine planes are tilted with respect to the helical axis. All the glycosidic angles of adenosines are anti with respect the sugar, as observed also in the poly r**A** single helix. Sugar puckers are found to be predominantly C2'-endo.

Using NMR, small angle X-ray scattering and viscosity measurements it has been shown that poly r**A** actually exists as a structured single helix [s17]. In line with these observation, we see that poly d$\mathbf{A}_{15}$ at pH 7 recapitulates the behavior of poly r**A**

experimentally. Further, MDS on the poly dA single strand showed a nicely structured helical form driven by stacking of the large aromatic faces of adenines (see SI-Figure 9 for helical parameters) which is also reflected experimentally in its CD spectrum.

MD Simulations on the protonated parallel, poly dA_{15} duplex:

The double helix was made using NAMOT 2 software and subjected to an MD simulation as described earlier. During the 20 ns simulation this duplex adopts and maintains a highly stable structure according to the model shown in SI-Figure 10. Interestingly, this duplex recapitulates perfectly the features of the poly r**A** double helix.

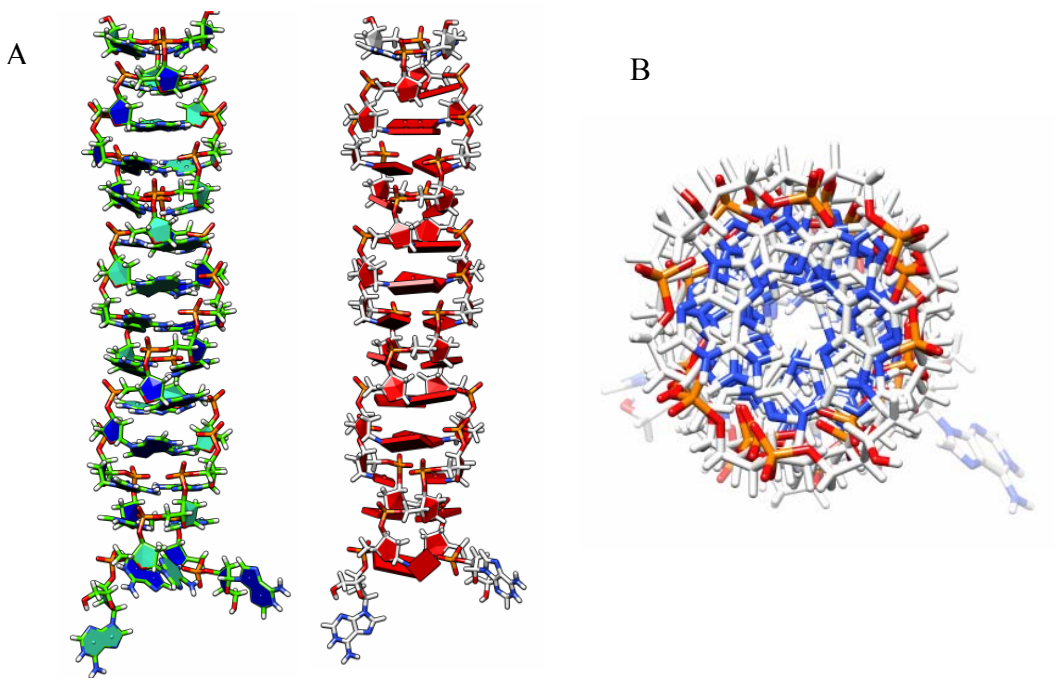

SI Figure 10: A) Two different representations of the structure of poly d$\mathbf{A_{15}}$ parallel, protonated double helix after 20 ns molecular dynamics simulation incorporating a distance restraint. **B**) End on view of this structure showing the characteristic phosphate periphery surrounding the hydrophobic base stacked region in DNA duplexes.

This duplex is considerably stretched toward its long axis and composed of symmetrical AH^+-H^+A base pairs. The helix is 8-fold; implying a ~45° turn angle per nucleotide and the pitch height is 31.2 Å. A dyad axis coincides with the helical axis which results in rotationally symmetric base pairs. Importantly, during the MD simulation, the perfectly

planar AH^+-H^+A base pairs in the model became tilted by ~ 12° with respect to horizontal to the helical axis – this is a characteristic feature of the base pairs in the poly r**A** duplex fiber diffracted structure. All the averaged helical parameters derived using CURVES 5.1 (s18) are listed below:

Backbone Torsion Angles: Local Inter-base parameters:

Chi	Gamma	Delta	Epsilon	Zeta	Alpha	Beta
-173.1	57.8	83.1	-153	-62.4	-69.2	-172.53

Shift	Slide	Rise	Tilt	Roll	Twist
0.03	-2.83	3.9	-13	-2.9	44.3

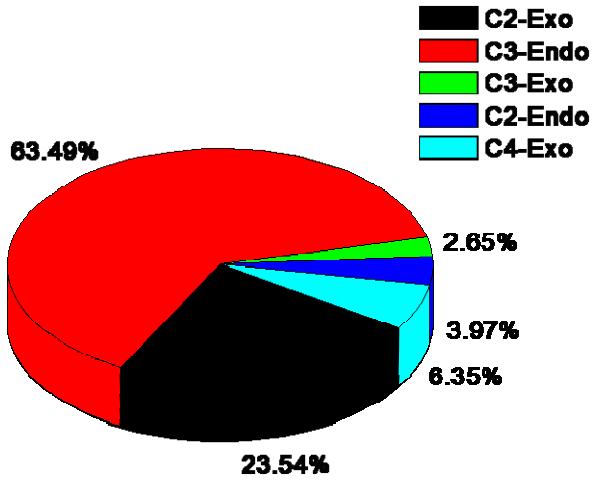

Minor Groove width	~ 5.1Å
Major Groove width	n.a
Intrahelical P-P distance	~ 6.5 Å
Helical Pitch	~31 Å
Rise	~ 3.7 Å
Helix diameter	~ 16 Å

SI Figure 11: A) Pie chart showing frequency of different types of sugar puckers in the poly d**A** duplex. **B**) Major global helical parameters are summarized in the table.

The parallel stranded poly d$\mathbf{A}_{15}$ duplex adopts an overall right handed helical twist. Certain regions in the duplex show more helical twist (>50°) than other regions both locally as well as globally, while the mean twist is found to be ~45°. The axial rise for each step is in the range of 3.3 to 4.6 Å for the poly dA duplex similar to the poly r**A** helix (~3.9 Å). The glycosidic torsion angles are anti and the sugar puckers are mostly N-

type. Most of the sugars adopt c3′-endo conformations but c2′-exo, c4′-exo conformations are also found (see SI Figure 11).

Base Pairing:

Notably, the MD simulated structure reveals that N1-H moves to within the H-bonding distance from the O2P for all base pairs (final distance after MD: 2.9 ± 0.3 Å, initial distance before MD: ~4 Å). A typical base pair is shown in SI Figure 12A. This is not unusual considering that oxygen possesses two lone pairs capable of simultaneously forming two H-bonds. In the poly r**A** duplex, the N1-H^+ and $^-$O-P has been described as a salt bridge that serves to bring the phosphate close to the helix axis in order to facilitate H-bond formation between N6-H1 and O2P.

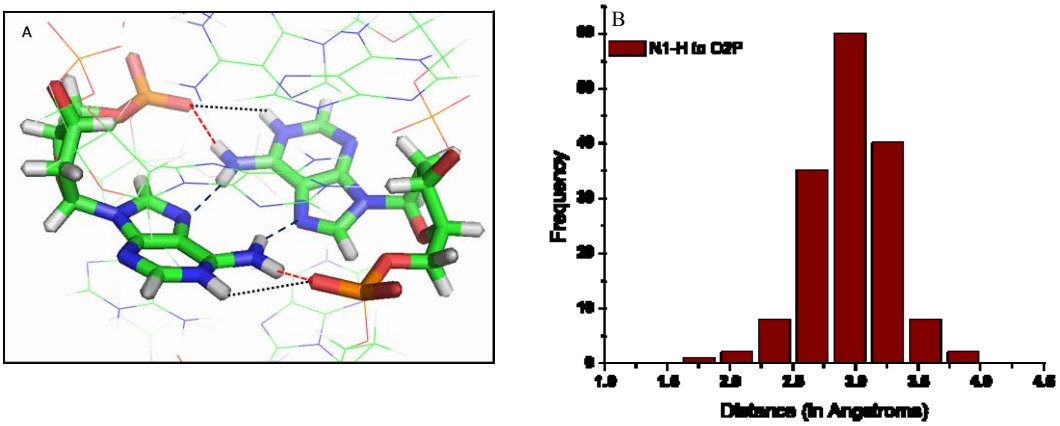

SI Figure 12: A) Base pairing scheme of AH^+-H^+A. (a) H-bond between N6-H2 and N7 shown by dotted blue line; (b) Strong proton-mediated interaction between N1-H and O2P (shown by dotted black line) considered also as an inner salt effect (c) H bond between N6-H1 and O2P, shown by dotted red line. **B**) Histogram showing the mean distance (in Å) between N1-H to O2P to be about 2.9 Å which is also ideal for H-bonding.

Even in poly d**A**, this inner salt effect is evident from the thermal stability studies (see salt dependence section in revised m/s) where the helix is destabilized with increasing ionic strength of the solution. However, the unusually high thermal stability of this duplex is in line with the extra strong proton-mediated interaction between N1-H^+ and $^-$O-P predicted by the MD simulation which would give rise to the equivalent of 6 H-

bonds per AH^+-H^+A base pair. This is also experimentally supported by the data on its dissociation kinetics. Structure formation due to protonation on N1 occurs on the millisecond time scale in line with the kinetics for protonation of any exposed site. However dissociation is substantially slower (in seconds) indicating reluctance for de-protonation at this site. This is in line with the proton at this site either being buried or held tightly by H-bonding. Thus, MD simulations combined with experimental data therefore suggests a possible additional role for the N1-H as an H-bond in addition to mediating an inner salt effect.

MD simulation on unprotonated duplex:

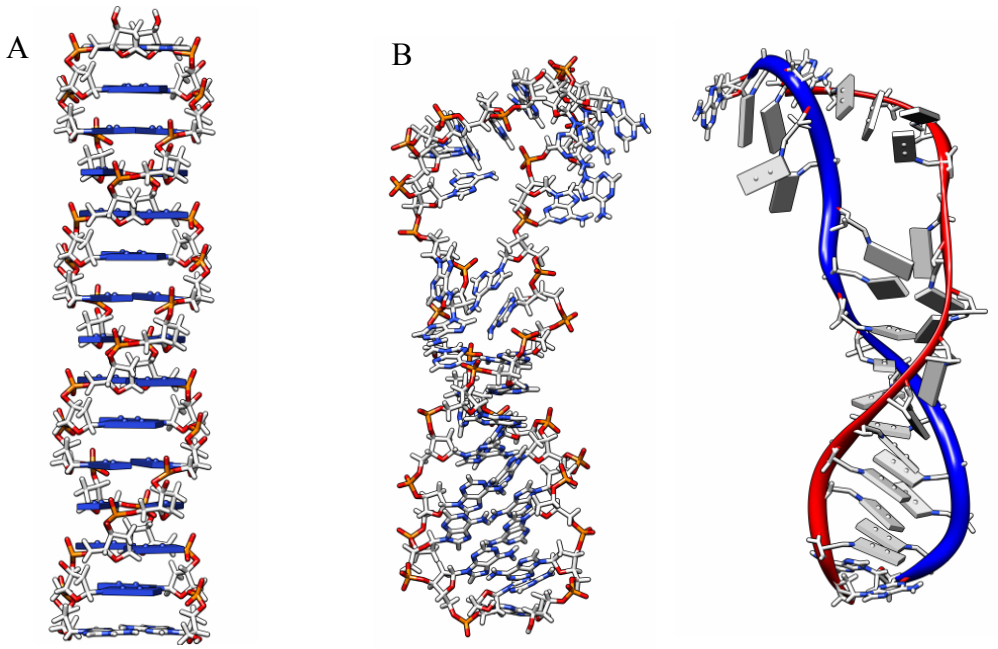

SI Figure 13: A) Model shows the starting structure for the MD simulation. Importantly, bases are not tilted with respect to the helix axis. **B)** Two different representations **of** structure of the unprotonated duplex after MD simulation. It shows a loose base pairing at the 3'-end.

It has been suggested (s3) that the protonation of adenines causes electrostatic stabilization of the poly r**A** parallel duplex and that without protonation this duplex is unstable. Our experiments reveal a similar role for the N1 protonation in the poly d**A** duplex as well, strongly supported by MD simulations. As a control, we performed MD

simulations on a parallel stranded poly d**A** duplex without N1 protonation. For this we constructed two kinds of parallel stranded poly d**A** duplexes with same pitch and rise as described for poly r**A**, where one had all C3'-endo sugar puckers and the other with all C2'-endo sugar puckers. In line with the proposed importance of N1 protonation, both these unprotonated duplexes were not stable (See SI-Figure 13). Although there is a dramatic departure from the initial structure, both strands did not collapse totally. There were regions at the 3′-end that were loosely associated, although the 5′ end is totally frayed. This certainly reaffirmed the role of N1-protonation in stabilization of the parallel duplex. It is likely to (i) bring the phosphate on the opposite strand closer to the helical axis (ii) electrostatically stabilize the helix by making the whole entity electrically neutral and (iii) increase the number of H-bonds per the AH^+-H^+A base pair (see SI- Figure 12A). Thus we delineate a structure of the poly d**A** double helix and for the first time constructed an atomistic model of the poly d**A** based on MD simulations. These suggest an additional role for N1 protonation to what has been described thus far.

Concentration and Length dependence of kinetics of poly d**A duplexation:**

In order to measure concentration dependence of the association d$\mathbf{A}_{15}$, kinetics experiments were performed using the fluorescence of 3′-TMR-d$\mathbf{A}_{15}$ which self-quenches due to duplex formation. To 20 μl of 0.50 μM, 1 μM and 2 μM 3′-TMR-d$\mathbf{A}_{15}$ in 100 μM phosphate buffer at pH 7, 5 μL of 50 mM pH 3 phosphate buffer was added to cause a pH jump to pH 3. Fluorescence of TMR-d$\mathbf{A}_{15}$ quenches due to duplex formation as shown in SI Figure 3A. The SI figure 14 A shows the self-quenching for TMR-d$\mathbf{A}_{15}$ at strand concentrations of 0.5 μM, 1.0 μM and 2.0 μM respectively. Clearly, the association is diffusion-limited as well as dependent on concentration, emphasizing the intermolecular nature of the duplex formation. These curves fitted well to a second order rate equation (s19) giving a second order rate constant of $k_{on} = (5.3 \pm 0.5) \times 10^7\ M^{-1}s^{-1}$ for all traces. This is further consistent with duplexation being bi-molecular.

To see the effect of length of d**A** tract on association, similar experiments were performed with dA_{10} and dA_{20} at 0.5 μM strand concentrations (SI figure 14B). With increase in A-tract length, the reaction is faster (SI Table 2), indicative of larger K_a for longer lengths of A-tracts in line with our expectations.

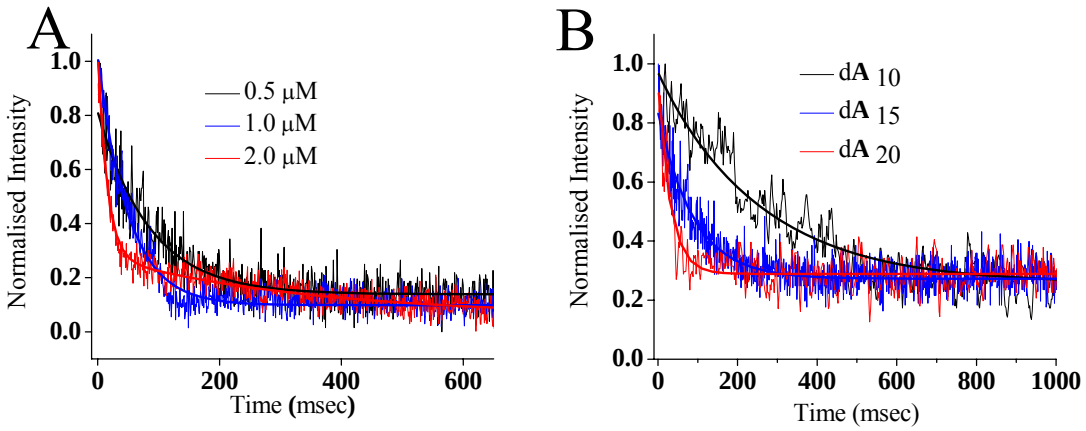

SI Figure 14: A) Concentration dependence of d$\mathbf{A}_{15}$ duplex formation. **B**) Kinetics of formation of poly d**A** duplex of different lengths at 0.5 μM concentration.

SI Table 2: Length dependence kinetics of poly d**A** segments

Length of poly d**A**	Association rate constant k_{on} ($M^{-1}s^{-1}$)
10	1.3×10^{7}
15	5.3×10^{7}
20	9.5×10^{7}

References:

s1**.** C.A. Bush & H.A. Scheraga, *Biopolymers*, **1969**, *7*, 395-409.

s2. J.L. Alderfer & S.L. Smith, *J. Am. Chem. Soc.* **1971**, *93*, 7305-7314.

s3. A. Rich, D. R. Davies, F. H. C. Crick, J. D. Watson, *J. Mol. Biol.* **1961**, *3*, 71-86.

s4. a) S.Bernacchi, Y. Mély, *Nucleic Acids Res*. **2001**, *29*, e62; b) S. Modi, A. H. Wani, Y. Krishnan, *Nucleic Acids Res*. **2006**, *34*, 4354-4363; c) S. Chakraborty, S. Modi, Y. Krishnan, *Chem. Commun*. **2008**, 70-72; d) S. Chakraborty & Y. Krishnan, *Biochimie*, **2008**, *90*, 1088-1095.

s5. G. G. Dvoryantseva, T. N. Ul'yanova, T. Ya. Filipenko, M. P. Nemeryuk, T. S. Safonova, Y. N. Sheinker, P. V. Petrovskii, E. I. Fedin, *Khim. Geterotsikl. Soedin*. **1977**, *1*, 49-54.

s6. M. W. Germann, N. Zhou, J. H. van de Sande, and H. J. Vogel, Methods in Enzymology, **1995**, *261*, 207-225.

s7. D.A. Case, D.A. Pearlman, J.W. Caldwell, T.E. Cheatham, W.S. Ross, C. Simmerling, T. Darden, K.M. Merz, R.V. Stanton, A. Cheng, J.J. Vincent, M. Crowley, V. Tsui, R. Radmer, Y. Duan, J. Pitera, I. Massova, G.L. Seibel, U.C. Singh, P. Weiner & P.A. Kollman, AMBER 8.0, 1999, University of California, San Francisco, CA. -.

s8. C.S. Tung and E.S. Carter, *CABIOS,* **1994**, *10*, 427.

s9. M.J. Frisch, G.W. Trucks, H.B. Schlegel, G.E. Scuseria, M.A. Robb, J.R Cheeseman, Jr. J.A. Montgomery, T. Vreven, K.N. Kudin, J.C. Burant, J.M. Millam, S.S. Iyengar, J. Tomasi, V. Barone, B. Mennucci, M. Cossi, G. Scalmani, N. Rega, G.A. Petersson, H. Nakatsuji, M. Hada, M. Ehara, K. Toyota, R. Fukuda, J. Hasegawa, M. Ishida, T. Nakajima, Y. Honda, O. Kitao, H. Nakai, M. Klene, X. Li, J.E. Knox, H.P. Hratchian, J.B. Cross, V. Bakken, C. Adamo, J. Jaramillo, R. Gomperts, R.E. Stratmann, O. Yazyev, A.J. Austin, R. Cammi, C. Pomelli, J.W. Ochterski, P.Y. Ayala, K. Morokuma, G.A. Voth, P. Salvador, J.J. Dannenberg, V.G. Zakrzewski, S. Dapprich, A.D. Daniels, M.C. Strain, O. Farkas, D.K. Malick, A.D. Rabuck, K. Raghavachari, J.B. Foresman, J.V. Ortiz, Q. Cui, A.G. Baboul, S. Clifford, J. Cioslowski, B.B. Stefanov, G. Liu, A. Liashenko, P. Piskorz, I. Komaromi, R.L. Martin, D.J. Fox, T. Keith, M.A. Al-Laham, C.Y. Peng, A. Nanayakkara, M. Challacombe, P.M.W Gill, B. Johnson, W. Chen, M.W. Wong, C. Gonzalez and J.A. Pople, Gaussian 03, Revision C.01, Gaussian, Inc., Wallingford CT, **2004**.

s10. J. Wang, W. Wang, P.A. Kollman, D.A. Case, *Journal of Molecular Graphics and Modeling*, **2006**, *25*, 247.

s11. P. Cieplak, W.D. Cornell, C. Bayly & P.A. Kollman, *J. Comp. Chem.* **1995**, *16,* 1357-1377.

s12. W.L. Jorgensen, J. Chandrasekhar, J.D. Madura, R.W. Impey and M.L. Klein, *J. Chem. Phys*. **1983**, *79*, 926–935.

s13. P. K. Maiti, T. A. Pascal, N. Vaidehi, et al. *Nucleic Acids Res.* **2004**, *32*, 6047.

s14. P. K. Maiti and B. Bagchi, *Nano.Letts*, **2006**, *6*, 2478.

s15. Y. Duan, C. Wu, S. Chowdhury, M.C. Lee, G. Xiong, W. Zhang, R. Yang, P. Cieplak, R. Luo, T. Lee, *J. Comput. Chem*. **2003**, *24*, 1999.

s16. U. Essmann, L. Perera, M. L. Berkowitz, et al., *J. Chem. Phys.* **1995**, *103*, 8577.

s17. a) W.K. Olson, *Nucleic Acids Res.* **1975,** *2*, 2055-2068; b) B.S. Stannard and G. Felsenfeld, *Biopolymers*, **1975**, *14*, 299-307.

s18. R. Lavery and H. Sklenar *J. Biomol. Struct. Dynam*. **1989**, *6*, 655-667.

s19. E. Carrillo-Nava, Y. Mejia-Radillo and H-J. Hinz, *Biochemistry*, **2008**, *47*, 13153-13157.